

Hydrothermal synthesis of uniform nanosized lithium-rich cathode material $\text{Li}_{0.94}[\text{Li}_{0.14}\text{Ni}_{0.26}\text{Mn}_{0.60}]\text{O}_2$ for high power lithium-ion batteries

Xueliang Li, Li Chen, Wenxiang He, Fangfang Peng, Zhenghui Xiao

Anhui Key Laboratory of Controllable Chemical Reaction and Material Chemical Engineering, School of Chemical Engineering, Hefei University of Technology, Hefei 230009, People's Republic of China
E-mail: xueliangli2005@163.com

Published in Micro & Nano Letters; Received on 19th October 2013; Revised on 21st November 2013; Accepted on 10th December 2013

A facile method of synthesising nanosized lithium-rich layered material with uniform particle size by a one-step hydrothermal approach has been developed. The effect of lithium ion concentration on hydrothermal products has been investigated. At low or high lithium ion concentration, products with poor layered characteristic were obtained. Under the optimum lithium ion concentration of 2.5 M, the obtained product has an $\text{Li}_{0.94}[\text{Li}_{0.14}\text{Ni}_{0.26}\text{Mn}_{0.60}]\text{O}_2$ stoichiometry with plate-like morphology and a uniform particle size of ~ 80 nm. The Brunauer-Emmett-Teller surface area measurement indicates that it possesses a surface area of $35.60 \text{ m}^2 \text{ g}^{-1}$. The electrochemical tests show that the as-prepared nanomaterial $\text{Li}_{0.94}[\text{Li}_{0.14}\text{Ni}_{0.26}\text{Mn}_{0.60}]\text{O}_2$ can acquire a high performance with an initial discharge capacity of 278 mAh g^{-1} at 30 mA g^{-1} and a corresponding capacity retention of 95% after 40 cycles. Moreover, it can even deliver 185 mAh g^{-1} at 1500 mA g^{-1} , exhibiting excellent rate capability which makes it suitable for high power lithium-ion batteries.

1. Introduction: Lithium-ion batteries (LIBs) are regarded as the most promising power sources for electric vehicles (EVs) and hybrid-electric vehicles (HEVs) owing to their high energy density, high power density and long lifetime [1–3]. To meet the demands, the development of new cathode materials with large capacity and high-rate capability is necessary [3–5]. Recently, lithium-rich (Li-rich) layered oxides have attracted widespread attention because of their extraordinarily high specific capacity ($\sim 250 \text{ mAh g}^{-1}$) [6–9] as compared with the current cathode materials such as LiCoO_2 , LiMn_2O_4 and LiFePO_4 . However, in spite of the capacity advantage, a rapid capacity fade occurs at higher C rates for this kind of material.

To overcome the shortcoming mentioned above, some efforts have been made to resolve the problem. Surface modification and fabrication of nanosized materials are demonstrated to be an effective means for improving the rate performance. Surface modification is a common method by coating inert or active materials, such as metal oxides [10–13], fluorides [14, 15] and phosphates [16] to improve the electrochemical performance of Li-rich layered oxides. However, it will cause a side reaction in some cases at a high operating voltage [13].

In contrast to surface modification, the fabrication of nanosized materials exhibits significant advantages in enhancing the rate capability, because a small diameter can lead to shorter diffusion paths in the particles and a more facile intercalation for lithium ions (Li^+). It is well known that a hydrothermal reaction is an effective route to acquire nanoparticles. For example, nanoplates $\text{Li}[\text{Li}_{0.17}\text{Ni}_{0.25}\text{Mn}_{0.58}]\text{O}_2$ with a thickness of 5–9 nm were prepared by a primary hydrothermal reaction and a subsequent calcination [17]. The as-prepared nanomaterial showed excellent rate performance and it exhibited reversible capacity at about 200 mAh g^{-1} at 6 C (1800 mA g^{-1}). Nanoparticles $\text{Li}_{0.93}[\text{Li}_{0.21}\text{Co}_{0.28}\text{Mn}_{0.51}]\text{O}_2$ with a size of 100 nm and a thickness of 20 nm were obtained by a two-step hydrothermal method, which showed a discharge capacity of about 216 mAh g^{-1} at 4 C (1000 mA g^{-1}) [18]. Thereafter, nanowires $\text{Li}[\text{Li}_{0.15}\text{Ni}_{0.25}\text{Mn}_{0.6}]\text{O}_2$ with a diameter of ~ 30 nm were prepared by a similar method. The electrochemical tests showed that it delivered 256 mAh g^{-1} at 7 C, exhibiting very excellent rate capability [19]. Nevertheless, none used the one-step hydrothermal method to prepare Li-rich material to our knowledge. Hence, to explore a straightforward approach for producing

nanomaterials is still necessary, since the hydrothermal process that possesses many scientific advantages, as illustrated above, is commonly complicated.

In this reported work, we have developed a one-step hydrothermal method to prepare Li-rich nanomaterials directly with a uniform particle size of ~ 80 nm, where MnSO_4 and NiSO_4 were used as the raw materials. In contrast to the hydrothermal strategies reported before, the present one in this Letter has a promoted advantage of simple operation in the whole process. A representational Li-rich layered oxide, $\text{Li}_{0.94}[\text{Li}_{0.14}\text{Ni}_{0.26}\text{Mn}_{0.60}]\text{O}_2$, was obtained by this approach and the charge–discharge tests showed that it could deliver capacities of 278 mAh g^{-1} at 0.1 C and 185 mAh g^{-1} at 5 C, respectively.

2. Experimental

2.1. Preparation of the samples: First, 0.811 g $\text{NiSO}_4 \cdot 6\text{H}_2\text{O}$ and 0.968 g $\text{MnSO}_4 \cdot \text{H}_2\text{O}$ were dissolved in 20 ml of distilled water, and then dropped into 50 ml of 2.5 M LiOH solution at about one drop per second under magnetic stirring at 60°C . After that 1.307 g $(\text{NH}_4)_2\text{S}_2\text{O}_8$ and an appropriate amount of LiNO_3 were added accompanied by constant stirring for about 1 min. Finally, the black suspension was transferred into a Teflon-lined stainless steel autoclave with about 80% fill rate (100 ml Teflon container) and thereafter sealed and heated at 200°C for 48 h. The obtained precipitate was separated by filtration and washed with distilled water several times and finally dried at 120°C for 24 h. The samples were named as LNMO-1, LNMO-2, LNMO-3 and LNMO-4 for the usages of 2.758, 5.516, 8.274 and 11.032 g of LiNO_3 , corresponding to the Li^+ concentrations 2.0, 2.5, 3.0 and 3.5 M in 80 ml solution, respectively.

2.2. Characterisation: Powder X-ray diffraction (XRD) was performed on a Japan Rigaku D/Max-rB diffractometer Cu-K α radiation ($\lambda = 0.15406 \text{ nm}$) between 10° and 70° . An inductively coupled plasma mass spectroscope (ICP, X Series 2, Thermo Fisher Scientific) was used to determine the metal contents. Field emission scanning electron microscopy (FESEM) studies were performed on SU8020 to observe the morphology of the samples. The Brunauer-Emmett-Teller (BET) surface area was measured on an automatic surface area and pore analyser (Micromeritics

Tristar II 3020 M). Field emission transmission electron microscopy (FETEM) was performed on JEM-2100F.

2.3. Electrochemical measurements: The electrochemical performances of the materials were tested by assembling CR2032 coin cells. The working electrode was fabricated by mixing homogeneously the active material, acetylene black and polyvinylidene fluoride in the weights of 80:10:10 with *N*-methyl-pyrrolidone. The electrolyte was a 1 M LiPF₆ solution in a mixed solvent of ethylene carbonate/dimethyl carbonate (1:1 v/v) and Celgard 2400 was used as the separator. The coin cells were assembled in a dry glove box filled with highly pure argon gas. The cell tests were performed on a BTS-55 Neware battery test system at 25°C between 2.0 and 4.8 V. Cyclic voltammetry (CV) tests were performed on an electrochemical workstation (CHI660B) at a scan rate of 0.5 mV s⁻¹ in the potential window of 2.0–4.8 V (against Li/Li⁺).

3. Results and discussion: The XRD patterns of the samples LNMO-1, LNMO-2, LNMO-3 and LNMO-4 are shown in Fig. 1. On the whole, the XRD patterns of all the samples are similar without an impurity phase. The Scherrer boarding of the reflections indicates that the as-prepared samples are nanosized and their diffraction peaks can be indexed to the α -NaFeO₂ structure with space group *R*-3 m. Since the radii of the Ni ions (Ni²⁺, 0.69 Å) and Li⁺ (0.76 Å) are similar, it was considered that Ni²⁺ and Li⁺ exchange between the 3b and the 3a sites (cation mixing) in this structure and that would give rise to disordering in the structure [20]. The peak intensity ratio *I*(003)/*I*(104) lines (*R*) was shown to measure the cation mixing and a value of *R* < 1.2 is an indicator of unfavourable cation mixing [21]. It is well known that the cation mixing will deteriorate the electrochemical performance of the Li-rich layered compounds because of the high concentration of inactive rock-salt domains in a layered solid matrix.

As shown in Fig. 1, the diffraction intensity of the peaks corresponding to the samples firstly increases and then decreases with the increasing of Li⁺ concentration. The values of *R* of LNMO-1, LNMO-2 and LNMO-3 are larger than 1.2, whereas the LNMO-4 (1.06) is the contrary, which indicates an unfavorable cation mixing in LNMO-4. At the low Li⁺ concentration of 2.0 M, the two major peaks corresponding to the (018) and the (110) peaks were merged (Fig. 1a). When the Li⁺ concentration increased to

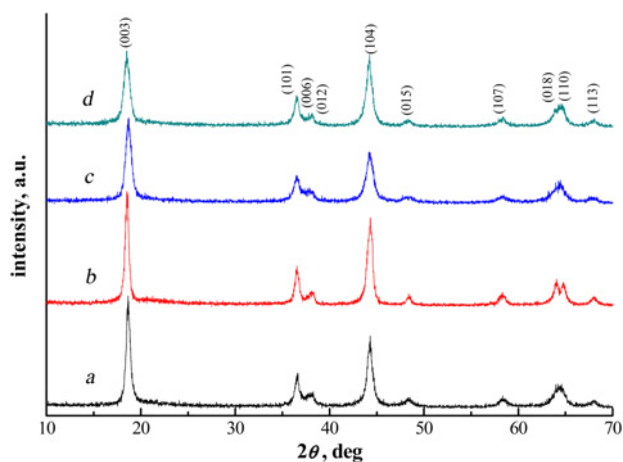


Figure 1 XRD patterns of the samples synthesised at various Li⁺ concentrations

- a Sample synthesised at 2.0 M Li⁺ concentration
- b Sample synthesised at 2.5 M Li⁺ concentration
- c Sample synthesised at 3.0 M Li⁺ concentration
- d Sample synthesised at 3.5 M Li⁺ concentration

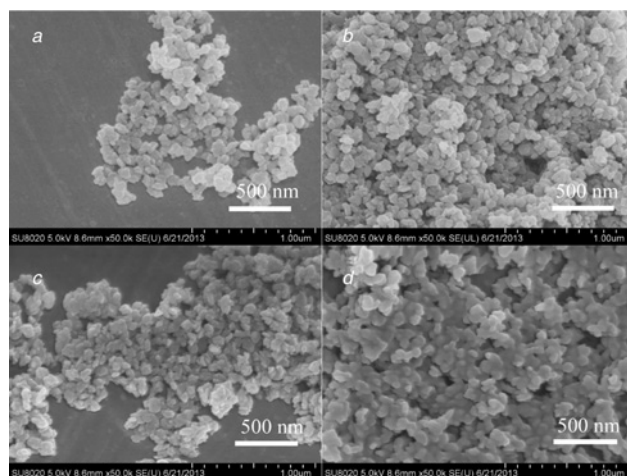


Figure 2 FESEM images of the samples synthesised at 200°C with different Li⁺ concentrations

- a Sample synthesised at 2.0 M Li⁺ concentration
- b Sample synthesised at 2.5 M Li⁺ concentration
- c Sample synthesised at 3.0 M Li⁺ concentration
- d Sample synthesised at 3.5 M Li⁺ concentration

2.5 M, the XRD pattern of LNMO-2 with the sharpest peaks was obtained (Fig. 1b). We can also observe the split of the (018) and the (110) peaks which are characteristic of the layer structure [20, 22]. This indicates that LNMO-2 has a typical well-formed layered structure. As the Li⁺ concentration continued to increase, the (018) and the (110) peaks merged again (Figs. 1c and d). These results indicate that the Li⁺ concentration plays a critical role in forming an ordered and well-formed layered structure Li-rich product. LNMO-2 presents a better layered structure and well-crystallisation, which will benefit the electrochemical properties. The ICP analysis results reveal that the LNMO-2 sample has an Li_{0.94}[Li_{0.14}Ni_{0.26}Mn_{0.60}]O₂ stoichiometry.

Fig. 2 is the FESEM image of all the samples prepared at 200°C with various Li⁺ concentrations. When the Li⁺ concentrations were 2.0 and 2.5 M, the products were non-agglomerated plate-like nanoparticles, and dispersed uniformly with a particle size of about 80 nm. However, as the Li⁺ concentration increased to 3.0 M, the nanosized gains began to aggregate. When the Li⁺ concentration was increased to 3.5 M, the particles aggregated seriously with a smooth surface. The BET-specific surface area of LNMO-2 is 35.60 m² g⁻¹.

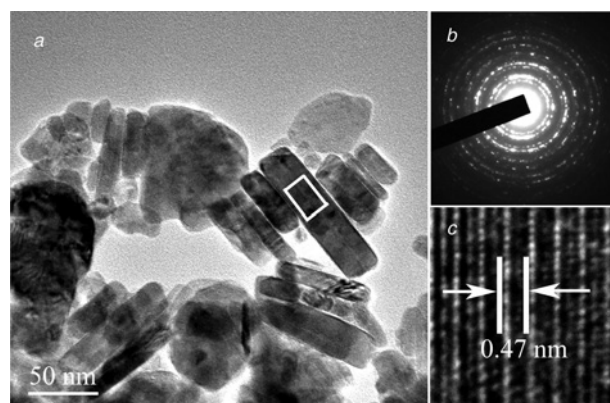


Figure 3 TEM image, HRTEM image and SAED pattern of sample LNMO-2, corresponding to Li_{0.94}[Li_{0.14}Ni_{0.26}Mn_{0.60}]O₂

- a TEM image
- b SAED pattern
- c HRTEM image corresponding to the white frame marked in Fig. 3a

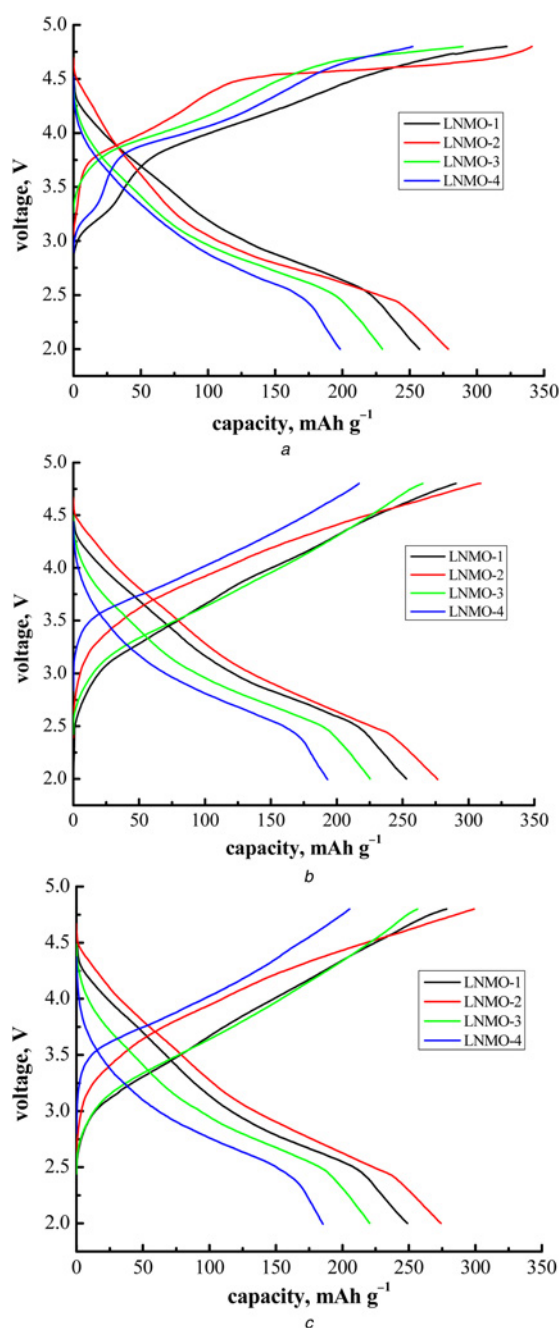


Figure 4 Charge–discharge curves of all the samples at 30 mA g^{-1} in the voltage range of 2.0–4.8 V
a First charge–discharge curves
b Fifth charge–discharge curves
c Tenth charge–discharge curves

As we all know, the electrochemical properties of the battery depend largely on the particle size, distribution of the particle size and the morphology of the electrode materials as well. The materials which have a smaller particle size tend to have high capacity, and uniform particle size distribution could result in enhancing the overall battery performance by the uniform depth of the charge and the discharge of each particle.

The as-prepared LNMO-2, corresponding to $\text{Li}_{0.94}[\text{Li}_{0.14}\text{Ni}_{0.26}\text{Mn}_{0.60}]\text{O}_2$, was further characterised by FETEM, as shown in Fig. 3. As we can see, the thickness of the nanoplates is about 20 nm, and a continuous interference fringe spacing (0.47 nm) can be observed clearly. From the results of our experiment, the nanoplates with thin thickness can acquire high rate performance.

Table 1 The discharge capacity for the first, fifth and tenth as-prepared samples

Sample	LNMO-1, mAh g^{-1}	LNMO-2, mAh g^{-1}	LNMO-3, mAh g^{-1}	LNMO-4, mAh g^{-1}
1st	257	278	229	198
5th	253	276	225	193
10th	249	274	220	185

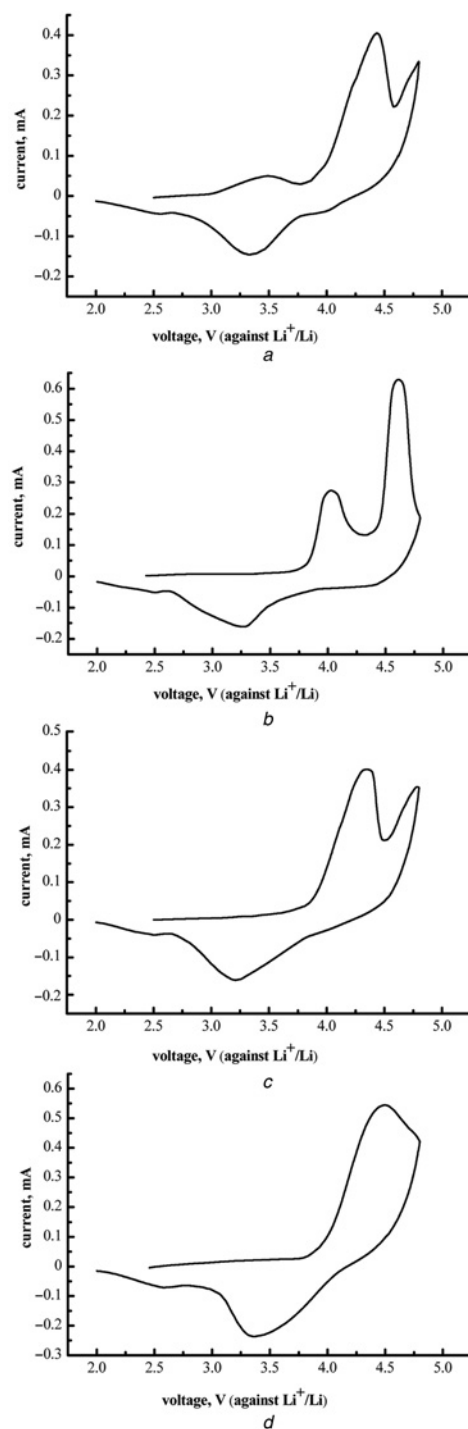


Figure 5 The initial CV curves scanned at 0.5 mV s^{-1} between 2.0 and 4.8 V
a Initial CV curve of LNMO-1
b Initial CV curve of LNMO-2
c Initial CV curve of LNMO-3
d Initial CV curve of LNMO-4

This could be ascribed to the short diffusion paths with the particles and more facile intercalation for the lithium ions.

Fig. 4 shows the first, the fifth and the tenth charge–discharge curves of all the samples at a current density of 30 mA g^{-1} in the voltage range of 2.0–4.8 V. It is evident that Fig. 4a is different from Figs. 4b and c. In the first charge curves, there is a slope at ca. 3.75 V in the first charge curves for all the samples, which is associated with the oxidation reaction of $\text{Ni}^{2+}/\text{Ni}^{3+}$ and/or $\text{Ni}^{2+}/\text{Ni}^{4+}$. The LNMO-2 sample has a long plateau at about 4.5 V, which is associated with the simultaneous removal of Li and O (as Li_2O) from the Li_2MnO_3 component [6]. In contrast, it does not appear in the other charge curves, which means that the other samples are not typical Li-rich layered material. It can be found that LNMO-2 possesses the highest specific discharge capacities of 278, 276 and 274 mAh g^{-1} after the first, the fifth and the tenth cycles, whereas LNMO-4 has the lowest capacity ca. 198, 193 and 185 mAh g^{-1} . It could be explained by the XRD results. The discharge capacity of all the as-prepared products for the first, the fifth and the tenth are listed in Table 1. It is worth noting that the discharge capacities of all the samples correspond with the XRD results very well.

CV tests were performed to further understand the initial charge–discharge curves for the four materials. Fig. 5 shows the initial CV curves of the four materials at a scan rate of 0.5 mV s^{-1} . As shown in Fig. 5, there are two anodic peaks in Figs. 5a–c, whereas only one anodic peak can be found in Fig. 5d. The anodic peak above 4.5 V in Figs. 5a–c is mainly associated with the irreversible electrochemical activation reaction for the removal of Li and O (as Li_2O) from the Li_2MnO_3 component to form MnO_2 [10].

Fig. 6a shows the cycle capability of $\text{Li}_{0.94}[\text{Li}_{0.14}\text{Ni}_{0.26}\text{Mn}_{0.60}]\text{O}_2$. From it we can see that the discharge capacities after the

first and the fortieth cycles were 278 and 264 mAh g^{-1} at 0.1 C (30 mA g^{-1}), respectively. The capacity retention after 40 cycles was about 95% which indicates that the as-obtained nanomaterial presents an excellent cycle capability and Fig. 6b is the rate capabilities of $\text{Li}_{0.94}[\text{Li}_{0.14}\text{Ni}_{0.26}\text{Mn}_{0.60}]\text{O}_2$. The sample delivered 278, 262, 244, 220 and 185 mAh g^{-1} at 0.1, 0.5, 1, 2 and 5 C, respectively, indicating excellent rate capabilities. This superior electrochemical performance can be ascribed to the well-formed layered structure and uniform particle size distribution in the nanoscale. As shown in Fig. 6b, the capacity decreased faster with the higher C rates. This phenomenon can be ascribed to the large polarisation at high current density.

4. Conclusion: Uniform nanoscale Li-rich layered cathode materials were successfully prepared via a one-step hydrothermal synthesis using MnSO_4 , NiSO_4 , $(\text{NH}_4)_2\text{S}_2\text{O}_8$, LiOH and LiNO_3 as the starting materials. We investigated the effect of the Li^+ concentration on the hydrothermal products systematically and found that the Li^+ concentration played a critical role in forming an Li-rich product with a good layered characteristic. Compared with the other samples, the sample synthesised at 2.5 M Li^+ concentration with an $\text{Li}_{0.94}[\text{Li}_{0.14}\text{Ni}_{0.26}\text{Mn}_{0.60}]\text{O}_2$ stoichiometry presents a uniform size of ca. 80 nm and a distinguished electrochemical performance. It can deliver 278 mAh g^{-1} at 30 mA g^{-1} and even 185 mAh g^{-1} at 1500 mA g^{-1} . Owing to this facility, it will be a promising approach for preparing high energy and high power Li-rich nanomaterials.

5. Acknowledgments: This work was supported by the Science and Technology Project of the Land and the Resources of Anhui Province (2011-k-11, 2012-k-25) and the Soft Science Project of the Land and the Resources of Anhui Province (2012021).

6 References

- [1] Gao X.-P., Yang H.-X.: ‘Multi-electron reaction materials for high energy density batteries’, *Energy Environ. Sci.*, 2010, **3**, (2), pp. 174–189
- [2] Su L., Jing Y., Zhou Z.: ‘Li ion battery materials with core-shell nanostructures’, *Nanoscale*, 2011, **3**, (10), pp. 3967–3983
- [3] Tarascon J.-M., Armand M.: ‘Building better batteries’, *Nature*, 2008, **451**, pp. 652–657
- [4] Sun Y.-K., Myung S.-T., Park B.-C., Prakash J., Belharouak I., Amine K.: ‘High-energy cathode material for long-life and safe lithium batteries’, *Nature Mater.*, 2009, **8**, pp. 320–324
- [5] Goodenough J.B.: ‘Cathode materials: a personal perspective’, *J. Power Sources*, 2007, **174**, (2), pp. 996–1000
- [6] Armstrong A.R., Holzappel M., Novak P., ET AL.: ‘Demonstrating oxygen loss and associated structural reorganization in the lithium battery cathode $\text{Li}[\text{Ni}_{0.2}\text{Li}_{0.2}\text{Mn}_{0.6}]\text{O}_2$ ’, *J. Am. Chem. Soc.*, 2006, **128**, (26), pp. 8694–8698
- [7] Gu M., Belharouak I., Zheng J., ET AL.: ‘Formation of the spinel phase in the layered composite cathode used in Li-ion batteries’, *ACS Nano*, 2013, **7**, (1), pp. 760–767
- [8] Thackeray M.M., Kang S.-H., Johnson C.S., Vaughey J.T., Benedek R., Hackney S.A.: ‘ Li_2MnO_3 -stabilized LiMO_2 (M = Mn, Ni, Co) electrodes for lithium-ion batteries’, *J. Mater. Chem.*, 2007, **17**, (30), pp. 3112–3125
- [9] Li G.R., Feng X., Ding Y., Ye S.H., Gao X.P.: ‘ AlF_3 -Coated $\text{Li}(\text{Li}_{0.17}\text{Ni}_{0.25}\text{Mn}_{0.58})\text{O}_2$ as cathode material for Li-ion batteries’, *Electrochim. Acta*, 2012, **78**, pp. 308–315
- [10] He W., Qian J., Cao Y., Ai X., Yang H.: ‘Improved electrochemical performances of nanocrystalline $\text{Li}[\text{Li}_{0.2}\text{Mn}_{0.54}\text{Ni}_{0.13}\text{Co}_{0.13}]\text{O}_2$ cathode material for Li-ion batteries’, *RSC Adv.*, 2012, **2**, (8), pp. 3423–3429
- [11] Seok Jung Y., Cavanagh A.S., Yan Y., George S.M., Manthiram A.: ‘Effects of atomic layer deposition of Al_2O_3 on the $\text{Li}[\text{Li}_{0.20}\text{Mn}_{0.54}\text{Ni}_{0.13}\text{Co}_{0.13}]\text{O}_2$ cathode for lithium-ion batteries’, *J. Electrochem. Soc.*, 2011, **158**, (12), pp. A1298–A1302
- [12] Wu Y., Manthiram A.: ‘Effect of surface modifications on the layered solid solution cathodes $(1-Z)\text{Li}[\text{Li}_{1/3}\text{Mn}_{2/3}]\text{O}_2$ -(Z) $\text{Li}[\text{Mn}_{0.5-y}\text{Ni}_{0.5-y}\text{Co}_{2y}]\text{O}_2$ ’, *Solid State Ionics*, 2009, **180**, (1), pp. 50–56

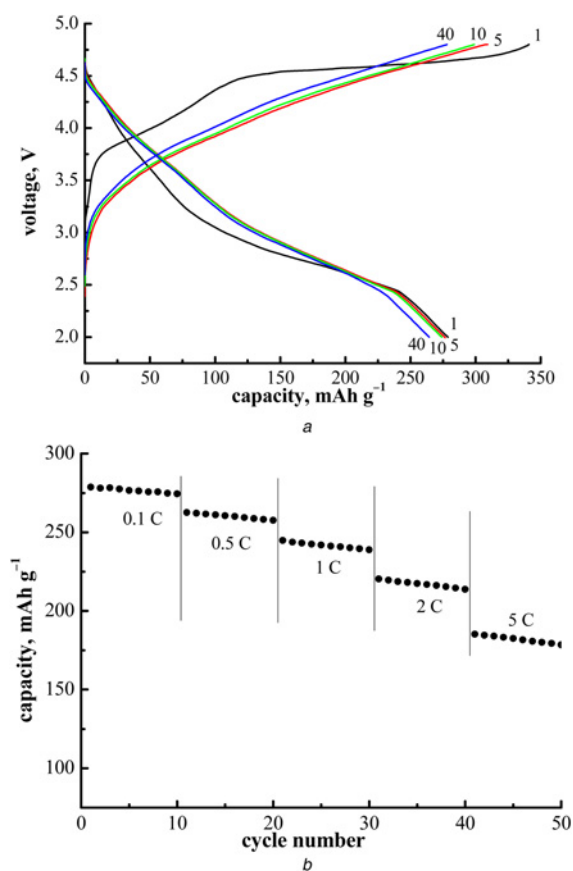


Figure 6 Electrochemical performance of $\text{Li}_{0.94}[\text{Li}_{0.14}\text{Ni}_{0.26}\text{Mn}_{0.60}]\text{O}_2$
a Cycle capability
b Rate capabilities (0.1 C = 30 mA g^{-1})

- [13] Liu J., Manthiram A.: 'Functional surface modifications of a high capacity layered $\text{Li}[\text{Li}_{0.2}\text{Mn}_{0.54}\text{Ni}_{0.13}\text{Co}_{0.13}]\text{O}_2$ cathode', *J. Mater. Chem.*, 2010, **20**, (19), pp. 3961–3967
- [14] Deng H., Belharouak I., Yoon C.S., Sun Y.K., Amine K.: 'High temperature performance of surface-treated $\text{Li}_{1.1}(\text{Ni}_{0.15}\text{Co}_{0.1}\text{Mn}_{0.55})\text{O}_{1.95}$ layered oxide', *J. Electrochem. Soc.*, 2010, **157**, (10), pp. A1035–A1039
- [15] Sun Y.K., Cho S.W., Lee S.W., Yoon C.S., Amine K.: 'AlF₃-coating to improve high voltage cycling performance of $\text{Li}[\text{Ni}_{1/3}\text{Co}_{1/3}\text{Mn}_{1/3}]\text{O}_2$ cathode materials for lithium secondary batteries', *J. Electrochem. Soc.*, 2007, **154**, (3), pp. A168–A172
- [16] Liu B., Zhang Q., He S., Sato Y., Zheng J., Li D.: 'Improved electrochemical properties of $\text{Li}_{1.2}\text{Ni}_{0.18}\text{Mn}_{0.59}\text{Co}_{0.03}\text{O}_2$ by surface modification with LiCoPO_4 ', *Electrochim. Acta*, 2011, **56**, (19), pp. 6748–6751
- [17] Wei G.-Z., Lu X., Ke F.-S., ET AL.: 'Crystal habit-tuned nanoplate material of $\text{Li}[\text{Li}_{1/3-2x/3}\text{Ni}_x\text{Mn}_{2/3-x/3}]\text{O}_2$ for high-rate performance lithium-ion batteries', *Adv. Mater.*, 2010, **22**, (39), pp. 4364–4367
- [18] Kim Y., Hong Y., Kim M.G., Cho J.: ' $\text{Li}_{0.93}[\text{Li}_{0.21}\text{Co}_{0.28}\text{Mn}_{0.51}]\text{O}_2$ nanoparticles for lithium battery cathode material made by cationic exchange from K-birnessite', *Electrochem. Commun.*, 2007, **9**, (5), pp. 1041–1046
- [19] Kim M.G., Jo M., Hong Y.-S., Cho J.: 'Template-free synthesis of $\text{Li}[\text{Ni}_{0.25}\text{Li}_{0.15}\text{Mn}_{0.6}]\text{O}_2$ nanowires for high performance lithium battery cathode', *Chem. Commun.*, 2009, 2, pp. 218–220
- [20] Shaju K.M., Subba Rao G.V., Chowdari B.V.R.: 'Performance of layered $\text{Li}(\text{Ni}_{1/3}\text{Co}_{1/3}\text{Mn}_{1/3})\text{O}_2$ as cathode for Li-ion batteries', *Electrochim. Acta*, 2002, **48**, pp. 145–151
- [21] Santhanam R., Rambabu B.: 'High rate cycling performance of $\text{Li}_{1.05}\text{Ni}_{1/3}\text{Co}_{1/3}\text{Mn}_{1/3}\text{O}_2$ materials prepared by sol-gel and co-precipitation methods for lithium-ion batteries', *J. Power. Sources*, 2010, **195**, (13), pp. 4313–4317
- [22] Kim H.-J., Jung H.-G., Scrosati B., Sun Y.-K.: 'Synthesis of $\text{Li}[\text{Li}_{1.19}\text{Ni}_{0.16}\text{Co}_{0.08}\text{Mn}_{0.57}]\text{O}_2$ cathode materials with a high volumetric capacity for Li-ion batteries', *J. Power. Sources*, 2012, **203**, pp. 115–120